Decentralized Adaptive-Virtual-Impedance-Based Predictive Power for Mismatched Feeders in Islanded Microgrids

Mubashir Hayat Khan*, Shamsul Aizam Zulkifli*‡, Ronald Jackson*, Elhassan Garba*, Nadia Zeb*

*Faculty of Electrical and Electronics Engineering, Universiti Tun Hussein Onn, 86400 Malaysia.

*University of Poonch Rawalakot AJ&K, FE&T, Department of Electrical Engineering.

(ge180116@siswa.uthm.edu.my, aizam@uthm.edu.my, he180095@siswa.uthm.edu.my, ge180033@siswa.uthm.edu.my, nadia.zeb@gmail.com)

‡ Corresponding Author: Shamsul Aizam Zulkifli, UTHM, Johor, 86400 Malaysia Tel: +60 123 487636, aizam@uthm.edu.my

Received: 28.01.2022 Accepted: 26.02.2022

Abstract- Islanded microgrids with mismatched feeder impedances have numerous limitations. For accuracy in power sharing, distributed generations (DGs) use conventional droop-based controls but do not consider the different line impedances connected to the DGs, which will affect the consumed power to the load. As known, the line impedance has effects on real power and reactive power in DGs, and hence line impedance parameters should be considered as part of a robust control mechanism in order to maintain the output voltage at the point of common coupling (PCC), while at the same time providing accurate power sharing. Therefore, this research proposed improved control algorithms combined with an adaptive-virtual-impedance-based decentralized predictive controller to solve these issues. An adaptive virtual impedance loop was added to the droop controller to increase power-sharing efficiency and maintain the voltage at the PCC. An improvement was also made on the inverter switching pattern for the prediction mechanism, where a multi-variable cost function was designed to replace the normally employed pulse-width modulation. The proposed control strategies were tested on an islanded microgrid system, which consisted of two DGs with different types of line impedances and with different rated power values for the loads. MATLAB/Simulink results showed that the proposed control strategy was able to give accurate power sharing based on the load demand and that the voltage at the PCC was maintained even with load changes.

Keywords Virtual impedance, Predictive control, Voltage stability, Droop-based control, Distributed generations (DGs), Mismatched line impedance

1. Introduction

The integration of renewable energy resources (RERs) is getting more and more consideration nowadays following the significant increase in oil prices and environmental concerns around the world [1]–[4]. Distributed generations (DGs) are starting to utilize RERs, such as solar energy, wind energy, etc., for electricity generation. Microgrids (MGs) are the most flexible electrical system in terms of control and are more reliable compared with traditional electrical power systems. MGs are considered to be an alternate electrical network in local distributions, but unfortunately there are still many control problems [5]–[8] that need to be addressed. This is because the control sections for MGs are divided into centralized and decentralized control topologies, where communication and non-communication control schemes are applied, respectively. Communication-less or decentralized droop control techniques are preferred because of their reliability and stability, in comparison with communication-based centralized control techniques. Moreover, the cost of communication links is the minimum in noncommunication techniques, which makes the decentralized control more cost-

effective as well [9]–[12]. Parallel DG inverters with different line impedances do not have accurate power sharing. So, the output impedance of each feeder is modified by adding a virtual impedance loop to equalize the output impedance of each feeder connected in parallel [13]–[15]. Generally, based on authors' observation, the proper estimation of line impedances is difficult to determine in virtual-impedance-based control schemes with mismatched feeder impedances. In [16], [17], centralized control strategies were used, which can adaptively tune the virtual impedance loops through an integrator. Moreover, the virtual impedance loop was designed for accurate reactive power sharing by considering frequency instabilities; however, the generation of the circulating current is the disadvantage of such control strategies. With mismatched impedances, the output voltage of the DG inverters is compensated by a secondary controller in centralized control schemes by considering a virtual impedance, as in [18], [19]. Nevertheless, the complex control algorithms of centralized secondary-communication-based techniques are practically difficult to implement.

In the droop-based decentralized control for a system with mismatched feeder impedances, a virtual impedance is added to the system to overcome power sharing issues and voltage drop [20], [21], in another research [22] dynamic droop based control applied to PV panels proposed for power control. A virtual-impedance-loop-based control for accurate reactive power sharing was suggested in [23]. An improved droop control was implemented, which can recover power-sharing precision, but voltage drop and frequency variations were not taken into an account. To attain constant voltage, virtual-impedance-based current harmonics suppression and voltage compensation control was used in [24]. The controller successfully compensated the voltage but accuracy in reactive power sharing was not realized in the control strategy. The investigation in [25] introduced the virtual-capacitor-algorithm-based control technique for accurate reactive power sharing. However, voltage deviations and errors in active power sharing were not addressed in the control schemes. Moreover, the accuracy in reactive power sharing was due to the absence of integral terms in the reactive power control loop. Therefore, a droop-based control combined with a virtual impedance loop was suggested in [26], where the P-ω droop control was implemented to enhance reactive power sharing; however, active power sharing and the load's active power were not accurate as per connected loads. In recent years, model-based predictive control schemes, such as finite control set model predictive control (FCS-MPC) and continuous control set model predictive control (CCS-MPC), have been applied in power converters' control schemes [27]–[29], where the advantage of the FCS-MPC over the CCS-MPC is the provision of a good response for applications with low switching frequencies [30], [31]. Power quality improvement in 5 Level converters and predictive control scheme presented in [32], [33]. Keeping in view the robustness of the FCS-MPC arctan droop-based scheme introduced in [34], the virtual impedance loop was inserted to ensure that power accuracy and voltage reference was generated by the modified droop control. The control strategy with the FCS-MPC arctan droop did not add details of voltage drop at the PCC that is caused by the addition of the virtual impedance loop. As virtual-impedance-based solutions in mismatched-feeder-impedance microgrid systems that creates voltage deviations, the researchers in [35] introduced a distributed predictive secondary controller to achieve power-sharing accuracy. However, the control scheme is very complicated and the computational burdened for the MPC restricts expandability.

In the conventional control scheme, voltage stability and power-sharing accuracy are not guaranteed when mismatched feeder impedances are connected to the system. Mostly, a static virtual impedance is added to the system, which compensates the feeder impedance mismatch to attain power-sharing accuracy, but the power shared by each DG inverter in parallel connection is not accurate as per connected load. Moreover, in FCS-MPC-based control schemes applied to power converters, while power-sharing accuracy and voltage regulation are achieved in the first-order system when tracking the voltage error signals for the second-order or higher-order system, voltage tracking errors occur and power sharing and voltage stability are not achieved at the PCC busbar. Therefore, this paper proposed an improved decentralized control via the FCS-MPC control scheme by using an adaptive virtual impedance (AVI) loop to ensure power-sharing accuracy and voltage stabilization, with the mismatched feeder impedances of the DGs connected in parallel. The proposed controller tracks the voltage and its derivative terms to minimize tracking errors. A cost function (CF) has been designed with the addition of conventional and derivative terms of the CF and also the AVI loop included. The proposed solution is applicable for mismatched-feeder-impedance microgrid systems with parallel-connected DG inverters. The proposed scheme utilizes two-step-ahead receding predictions to minimize computational burden and is equally effective in the second- or higher-order system as in the first-order system.

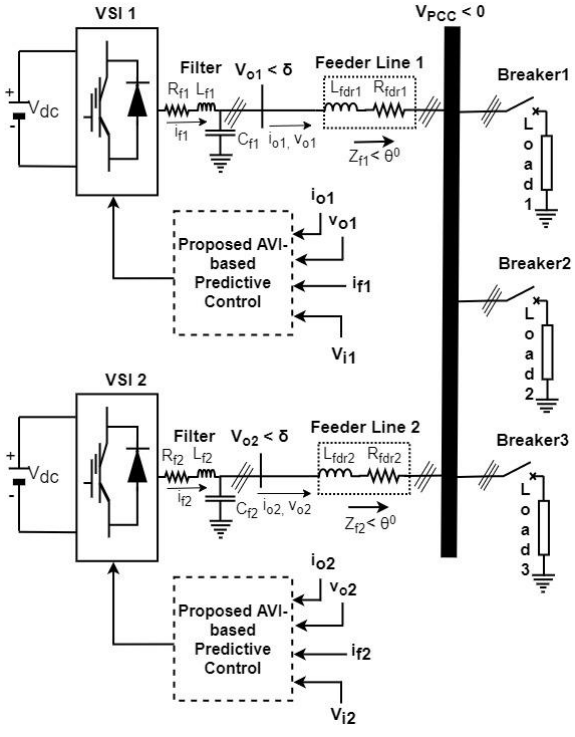

Fig. 1. Microgrid system with two VSIs

The FCS-MPC-based control scheme with the adaptive virtual impedance (virtual-impedance-based predictive controller) was applied to an islanded microgrid with two DGs. The three-phase microgrid system under study, comprising two same-rated voltage-source inverters (VSIs), a fixed DC voltage source, low-pass filters (LPFs), feeder lines and a common three-phase RL load connected at the PCC, is shown in Fig. 1.

This paper is arranged as follows: Section 1 presents the literature review and a short description of the microgrid system, which consisted of two identical voltage-source inverters, as well as an introduction of the proposed control. Section 2 presents the proposed FCS-MPC virtual-impedance-based predictive control scheme, while the power droop control, adaptive virtual impedance, LC filter and discretization are discussed in Section 3, the cost function and the weighting factor are discussed in Section 4. The result and discussion are presented in Section 5 and the conclusion is given in Section 6.

2. Proposed Control Scheme with Virtual Impedance Based on FCS-MPC

The proposed control scheme consisted of a droop control with an adaptive virtual impedance loop. The proposed control system for two DG inverters connected in parallel was based on the FCS-MPC technique, where an adaptive virtual impedance loop was applied to enhance power-sharing accuracy. Moreover, a voltage controller was added to the system to compensate the voltage drop during load variation. Fig. 2 shows the schematic diagram of a control system with a single DG.

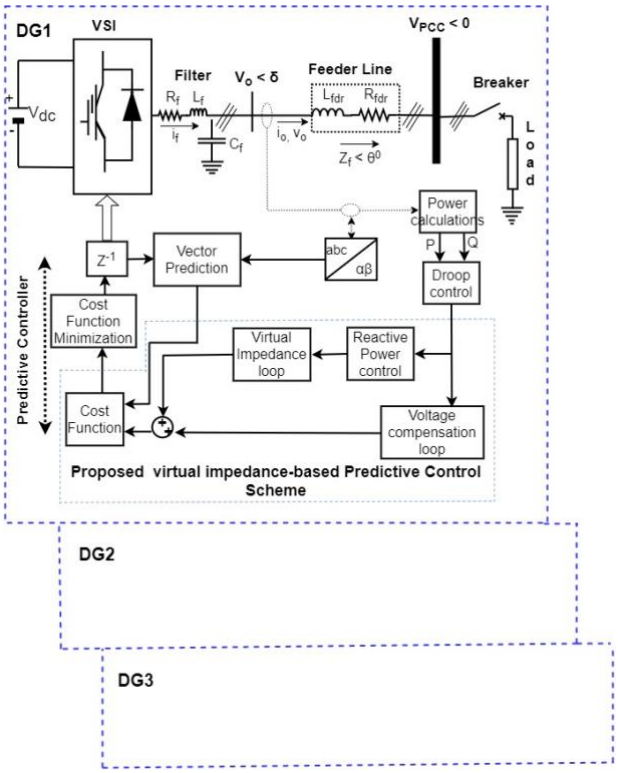

Fig. 2. Control system based on virtual impedance with single DG arrangement

The active power and reactive power for an islanded MG shown in Fig. 3 are given as:

$$P_i = \frac{V_i^2}{Z_{oi}}\cos\delta_i - \frac{V_i.V_{PCC}}{Z_{oi}}\cos(\theta_i + \delta_i) \quad (1)$$

$$Q_i = \frac{V_i^2}{Z_{oi}}\sin\theta - \frac{V_i.V_{PCC}}{Z_{oi}}\sin(\theta + \delta) \quad (2)$$

Where P_i and Q_i are active power and reactive power, respectively, and V_i (i =1, 2, 3, …) and VPCC are the VSI's voltage and the voltage at the PCC, respectively, while θ_i and δ_i are power angles. For higher X/R ratios, the dominant grid impedance is inductive and θ=90º, and so Equations (1) and (2) are written as:

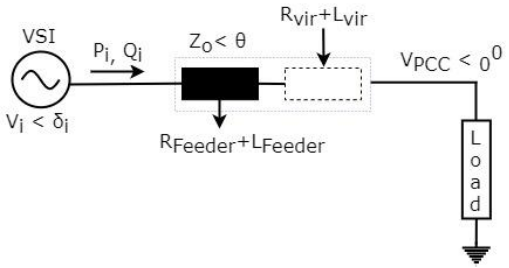

Fig. 3. VSI with feeder and virtual impedances

$$P = \frac{V_i V_{PCC}}{Z}\sin\delta \quad (3)$$

$$Q = \frac{V_i^2}{X} - \frac{V_i V_{PCC}}{X}\cos\delta \quad (4)$$

The relationships between P, Q and the droop for the islanded microgrid with V_{ref}, ω_{ref} and droop coefficients k_P, k_Q are expressed in the following equations:

$$V_{ref} = V_{nom} - k_P P_{cal} \quad (5)$$

$$\omega_{ref} = \omega_{nom} + k_Q Q_{cal} \quad (6)$$

3. Adaptive Virtual Impedance for Mismatched-Impedance Model

As mentioned, the difference between line impedances is mitigated through the addition of a virtual impedance. In most cases, the constants for the virtual impedances are added by assuming the line impedance of the system as either resistive or inductive. For example, in a resistive dominant feeder impedance, the virtual impedance's value is taken between 5 Ω to 30 Ω for low and medium line impedances in MG systems [36], [37]. The adaptive virtual impedance concept was implemented in the present study to address the aforementioned issues, with the aim of giving accurate power sharing among the DGs. The total impedance of the system after the addition of the adaptive virtual impedance is given as:

$$Z_{i\_total} = Z_{i\_feeder} + Z_{i\_virtual} \quad (7)$$

Where Z_{i_total} is the total impedance of the ith feeder, while $Z_{i\_feeder}, Z_{i\_virtual}$ are the physical feeder impedance and the virtual impedance, respectively. The voltage reference after adding the virtual impedance loop is modified as:

$$V^*_{ref\_AVI} = V_{o,ref} - v_v = V_{o,ref} - Z_v.I_{output} \quad (8)$$

$$V^*_{ref\_AVI} = V_{o,ref} - [(R_{i\_vir}) + (L_{i\_vir})]i_o \quad (9)$$

$$V^*_{ref\_AVI} = V_{o,ref} - R_{vir}i_o - L_{vir}\frac{di_o}{dt} \quad (10)$$

$$\begin{bmatrix} v_d \\ v_q \end{bmatrix}_{ref\_AVI} = \begin{bmatrix} v_d \\ v_q \end{bmatrix}_{o,ref} - R_{vir}\begin{bmatrix} i_{od} \\ i_{oq} \end{bmatrix} - L_{vir}\begin{bmatrix} -\omega i_{od} \\ \omega i_{oq} \end{bmatrix} \quad (11)$$

$$\begin{bmatrix} V_{d\_inv} - V_{0d} \\ V_{q\_inv} - V_{oq} \end{bmatrix} = \begin{bmatrix} (R_{feeder} + R_{vir}) & -\omega(L_{feeder} + L_{vir}) \\ \omega(L_{feeder} + L_{vir}) & (R_{feeder} + R_{vir}) \end{bmatrix}\begin{bmatrix} i_{od} \\ i_{oq} \end{bmatrix} \quad (12)$$

Where R_{vir} and L_{vir} are virtual impedance and virtual inductance, respectively, while $R_{total} = R_{feeder} + R_{vir}$ and $L_{total} = L_{feeder} + L_{vir}$ for complex impedances of the feeder. At steady state, the system response considering the droop equations is expressed as:

$$\begin{bmatrix} v_d \\ v_q \end{bmatrix}_{ref\_AVI} = \begin{bmatrix} v_d \\ v_q \end{bmatrix}_{o,ref} - \begin{bmatrix} R_{vir} & -\omega L_{vir} \\ \omega L_{vir} & R_{vir} \end{bmatrix}\begin{bmatrix} i_{od} \\ i_{oq} \end{bmatrix} \quad (13)$$

The P and Q from Equations (3) and (4) in the islanded MG with the new updated voltage in the dq reference-frame by using the AVI can be formulated as:

$$\begin{bmatrix} P \\ Q \end{bmatrix} = \begin{bmatrix} v_d & v_{oq,ref} \\ v_q & -v_{od,ref} \end{bmatrix}\begin{bmatrix} i_{od} \\ i_{oq} \end{bmatrix} \quad (14)$$

$$\begin{bmatrix} V_{d\_inv} - V_{od\_ref} \\ V_{q\_inv} - V_{oq\_ref} \end{bmatrix} = \frac{1}{v_d}\begin{bmatrix} (R_{feeder} + R_{vir}) & \omega(L_{feeder} + L_{vir}) \\ \omega(L_{feeder} + L_{vir}) & -(R_{feeder} + R_{vir}) \end{bmatrix}\begin{bmatrix} P \\ Q \end{bmatrix} \quad (15)$$

$$\begin{bmatrix} V_{id\_PCC} \\ V_{iq\_PCC} \end{bmatrix} = \begin{bmatrix} V_{PCC} - K_{qi}Q_i \\ 0 \end{bmatrix} - \frac{1}{v_{id}}\begin{bmatrix} (R_{ifeeder} + R_{vir}) & \omega_i(L_{ifeeder} + L_{ivir}) \\ \omega_i(L_{ifeeder} + L_{vir}) & -(R_{ifeeder} + R_{ivir}) \end{bmatrix}\begin{bmatrix} P_i \\ Q_i \end{bmatrix} \quad (16)$$

The voltage at the PCC can be modified by adding a new voltage reference obtained from the virtual impedance loop as per the connected RL load in the islanded MG system, where *Q* is shared equally and accurately in the system with parallel-connected DG inverters, as in the proposed controller. The voltage is compensated as:

$$\begin{bmatrix} V_{id\_PCC} \\ V_{qi\_PCC} \end{bmatrix} = \begin{bmatrix} V_o - K_{qi}Q_i \\ 0 \end{bmatrix}, V_{id\_PCC} - V_o = K_{qi}Q_i \quad (17)$$

$$Q_i = \frac{V_{id\_PCC} - V_o}{K_{qi}} \quad (18)$$

From Fig. 2, it is clear that $i_c = i_f - i_o$ and also $C_f.\frac{d}{dt}(V_{PCC}) = i_f - i_o$, and by considering the LC filter's current and voltage:

$$\frac{dv_{PCC}}{dt} = \frac{1}{c_f}(i_f - i_o) \text{ and } v_{inv} = v_f + i_f R_f + v_{PCC} \quad (19)$$

$$L_f\frac{di_f}{dt} = v_{inv} - v_{PCC} - i_f R_f \quad (20)$$

$$V^*_{ref\_AVI} = V_{o,ref} - R_{vir}i_o - L_{vir}\frac{di_o}{dt} \quad (21)$$

$$\frac{di_f}{dt} = \frac{1}{L_f}(v_{inv} - v_{PCC} - i_f R_f) \quad (22)$$

The continuous state-space model of the LC filter can be written as:

$$\frac{dx}{dt} = Ax + B_1 v_{inv} + B_2 i_{load} \quad (23)$$

where:

$$x = \begin{bmatrix} i_f \\ v_{PCC} \end{bmatrix}, A = \begin{bmatrix} -\frac{R_f}{L_f} & -\frac{1}{L_f} \\ -\frac{1}{c_f} & 0 \end{bmatrix}, B_1 = \begin{bmatrix} \frac{1}{L_f} \\ 0 \end{bmatrix} \text{ and } B_2 = \begin{bmatrix} 0 \\ -\frac{1}{c_f} \end{bmatrix}$$

Using Euler's forward approximation method suggested in [29] for prediction-based control and taking sampling time T_s for the predicted values of voltage and current:

$$\frac{dx}{dt} = \frac{x(k+1) - x(k)}{T_s} \text{ and } x(k+1) = A_d x(k) + B_d v_{inv}(k) \quad (24)$$

Where $A_d = e^{AT_s}$ and $B_d = \int_0^{T_s} e^{A\tau}Bd\tau$. Sampling time T_s was very small, which was 12e^{-6} s; hence, by approximation, $e^{AT_s} \approx 1 + AT_s$. The discrete values for $v_{PCC}(k), i_f(k)$ and $i_{load}(k)$ in the predictive controller utilized for the prediction of the capacitor's voltage in real α and imaginary β reference-frames are:

$$V_{PCC,\alpha\beta}(k+1) = V_{PCC,\alpha\beta}(k) + \frac{T_s}{c_f}\left(i_{f,\alpha\beta}(k) - i_{o,\alpha\beta}(k)\right) \quad (25)$$

$$i_{f,\alpha\beta}(k+1) = i_{f,\alpha\beta}(k) + \frac{T_s}{L_f}\left(v_{inv,\alpha\beta}(k) - V_{PCC,\alpha\beta}(k)\right) - \frac{R_f.T_s}{L_f} i_{f,\alpha\beta}(k)) \quad (26)$$

Likewise, the next execution, $(k+2)$, of the prediction can be calculated for $v_{PCC}(k), i_f(k)$ and $i_o(k)$.

4. Cost Function and Weighting Factor for Switching Pattern

The fundamental objective of the FCS-MPC is to determine the cost function and its minimization. A multi-functioned cost function for the proposed AVI-based predictive controller was proposed for the control scheme by taking the sum of the conventional cost function and the derivation of voltage and current of the LC filter. Moreover, the control scheme did not use the pulse-width modulation (PWM) signal generation anymore. The switching signals were generated by the combination of six switching patterns with three gate signals (S_a, S_b, S_c), utilizing the DC voltage source for each VSI [38].

The conventional multi-variable cost function (CF) has a single objective for the filter's voltage and current:

$$J_{conv} = \sum_{i=k}^{k+N-1} \left\| v_{ferror}(i) \right\|_2^2 + h_{\lim} + \lambda_u sw^2(i)) \quad (27)$$

Where $v_{ferror}(i)$ is the predicted tracking error, $h_{\lim}(i)$ is the current constraint and $sw^2(i)$ is the switching effort controlled by λ_u (weighting factor). The prediction error is expressed as $v_{ferror}(i) = v_f^*(i) - v_f(i)$, where $h_{\lim}(i) = 0$ when $i_f(i) \le i_{\max}$ and $h_{\lim}(i) = \infty$ when $i_f(i) > i_{\max}$, and the switching effort with the weighting factor is expressed as $sw(i) = \sum(u(i) - u(i-1))$.

The CF, by taking the derivatives of the filter's voltage and current in the αβ reference frame, is obtained as:

$$J_{derivative} = (C_f.\omega_{ref}.v_{f\beta}^* - i_{f\alpha} + i_{o\alpha})^2 + (C_f.\omega_{ref}.v_{f\alpha}^* - i_{f\beta} + i_{o\beta})^2 \quad (28)$$

Finally, the CF for the proposed AVI-based predictive control scheme can be derived as:

$$J_F = J_{conv} + \lambda_d J_{derivative} + h_{\lim} + \lambda_u sw^2 \quad (29)$$

The weighting factor for the proposed controller to tune the controller was adjusted as 0.05 and 0.002 using the trial-and-error method.

Fig. 4 shows the cost function's calculation flow for the proposed controller with voltage and *Q*-sharing compensation loop for DG_1. The same structure was used for DG_2. The voltage reference is generated from the conventional droop control and modified using the adaptive virtual impedance loop. As in conventional or static virtual-impedance-based controllers, the voltage at the PCC is not maintained when loads are added to the system, and hence compensation loops are added to maintain the voltage at the PCC busbar in mismatched-feeder-impedance microgrids. Nevertheless, power-sharing accuracy is guaranteed as per connected loads. The voltage reference from the conventional droop control is modified by the voltage compensation loop; at the same time, a reactive power sharing compensation loop is added to the system using the virtual impedance loop. The voltage compensation loop can track the nominal voltage and keeps the voltage at the PCC in the permissible range when loads are added to the system. Moreover, accuracy in *Q* sharing and *Q* load at the PCC is achieved through the adaptive virtual impedance loop designed for mismatched-feeder-impedance microgrid systems.

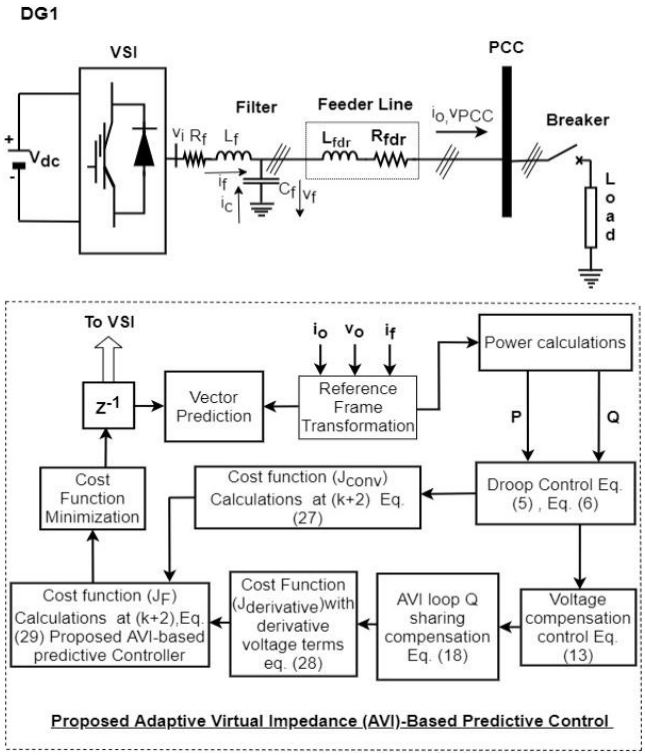

Fig. 4. Cost function for AVI-based control

The new voltage reference generated by the voltage compensation and the *Q* sharing compensation loops is then added to the cost function of the derivative voltage terms for further calculations. The switching signals generated by the switching sequence are utilized to calculate the cost function for each input value from (J_0,...,J_7) and the least-valued CF (J) is taken for the control action of the AVI-based FCS-MPC controller.

Table 1 shows the parameters for the proposed control scheme. The parameters applied to the islanded microgrid system with AVI-based predictive control scheme. Two identical DG inverters are connected in parallel and the control scheme is applied to each DG inverter separately. The power sharing and voltage deviation issues with mismatched feeder impedance is addressed in this research based on given parameters.

Table 1. System and control parameters

Parameters	Values
Nominal frequency	50 Hz
Filter inductor	3.3 mH
Feeder1 impedance	0.19 Ω, 2.8 mH
Feeder2 impedance	0.23 Ω, 3.14 mH
Droop coefficients	0.001, 0.001
Nominal voltage	220 V
$Load_1$	1200 W, 550 Var
$Load_2$	1000 W, 450 Var
$Load_3$	750 W, 150 Var
DC voltage	600 V
Filter capacitor	20 μF

5. Simulation Results

The Simulink models for the two DG inverters connected in parallel shown in Fig. 1 were designed by using MATLAB software. The overall control scheme consisted of decentralized control, and the simulation results of the mismatched feeder impedances of the islanded MG system in terms of sharing accuracy between *P* and *Q* at different connected loads are explained below. Moreover, the simulation results were compared with the fixed/static-virtual-impedance (SVI)-based control scheme where a designer's defined fixed virtual impedance was added to the system to overcome the feeder mismatch impedance, as explained in Section 3.

In the case of mismatched feeder impedances, the control system must ensure power-sharing accuracy for common connected loads. As shown in Fig. 5(a), from 0 s to 2 s, three different loads were applied to the system and the DG inverters were sharing equal power when connected to the loads. When $Load_1$ (1200 W, 550 Var) was connected to the system from 0 s to 0.6 s, DG_1 and DG_2 were sharing 600 W each and the total *P* received at the PCC was measured as 1200 W, as shown in the zoomed images in Figs. 5(b) and (e), respectively. From 0.6 s to 1.3 s, when $Load_2$ (1000 W, 450 Var) was connected, the zoomed images in Figs. 5(c) and (f) show that each DG inverter was sharing 1100 W and the total *P* at the PCC was received at 2200 W, respectively. As shown in the zoomed images in Figs. 5(d) and (g) for $Load_3$ (750 W, 150 Var), each DG inverter was sharing 1475 W and the total *P* at the PCC was measured as 2950 W, respectively. It can be seen both the DG inverters, which were connected in parallel in the proposed controller, were sharing accurate and equal *P* whenever there were mismatched feeder impedances between the DGs and the PCC busbar of the microgrid.

In the case of mismatched feeder impedances, the same loads as in the proposed control scheme were applied to the static-virtual-impedance-based control scheme at same time interval.

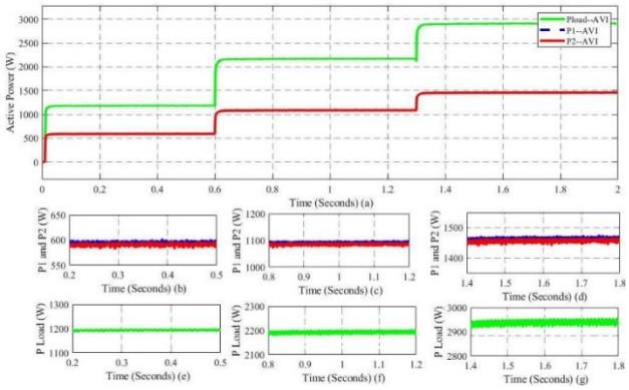

Fig. 5. Active power sharing and total *P* at PCC in proposed control scheme

The active power shared by each DG inverter in SVI control scheme for $Load_1$ is 500 W and the total active power received at the PCC was 1000 W, as shown in Figs. 6(b) and (e). When $Load_2$ was added to the system, the active power shared from DG_1 and DG_2 was 800 W and the total active power measured at the PCC was 1600 W, as shown in the zoomed images in Figs. 6(c) and (f). After adding $Load_3$, the active power shared by each DG inverter was 995 W; at the same time, the total active power at the PCC was 1990 W, as shown in Figs. 6(d) and (g). The simulation results clearly show that the proposed control scheme was sharing equal and accurate active power compared with the SVI-based control scheme as per connected load.

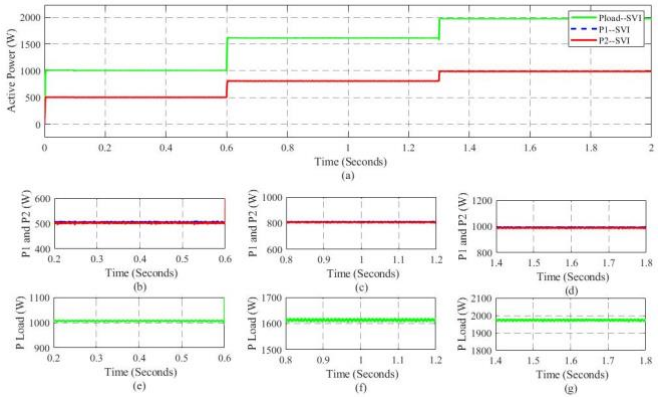

Fig. 6. Active power sharing and total *P* at PCC in static-virtual-impedance control scheme

Reactive power Q_1, reactive power Q_2 and the total *Q* received at the PCC in the mismatched islanded microgrid are shown in Fig. 7(a). As for $Load_1$ (1200 W, 550 Var), $Load_2$ (1000 W, 450 Var) and $Load_3$ (750 W, 150 Var), as shown in the zoomed images in Figs. 7(b), (c) and (d), DG_1 and DG_2 shared 275 Var, 500 Var and 575 Var for $Load_1$, $Load_2$ and $Load_3$, respectively, which were equal and accurate as per the connected load.

The values of total reactive power received at the PCC were 550 Var, 1000 Var and 1150 Var with the connected loads at different time intervals, as shown in Figs. 7(e), (f) and

(g). It was clear from the simulation results that accurate reactive power was shared in the proposed control scheme.

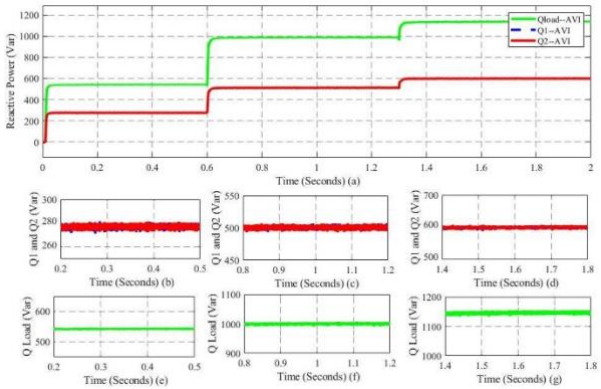

Fig. 7. Reactive power sharing and total *Q* at PCC in proposed control scheme

In the case of SVI-based control scheme for $Load_1$ (1200 W, 550 Var), $Load_2$ (1000 W, 450 Var) and $Load_3$ (750 W, 150 Var), the reactive power at different time intervals shared by each DG inverter is shown Fig. 8(a). When $Load_1$ is connected to the system, the reactive power shared by each DG inverter was 233 Var and the total reactive power at the PCC was 466 Var. After the addition of $Load_2$ and $Load_3$, the reactive power shared by each DG inverter was 370 Var and 400 Var, respectively, as shown in Figs. 8(c) and (d), whereas the total reactive power at the PCC was measured as 735 Var and 770 Var, respectively, as shown in Figs. 8(f) and (g).

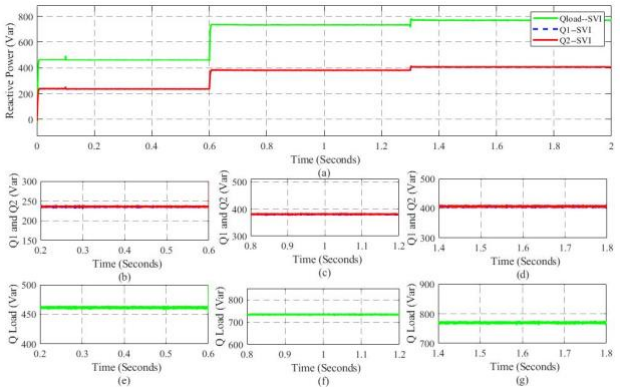

Fig. 8. Reactive power sharing and total *Q* at PCC in static-virtual-impedance control scheme

Fig. 9(a) shows the voltage at the PCC during load changes. It shows that the voltage was constant during the changes. Figs. 9(b), (c) and (d) are the zoomed images when the loads were applied. For $Load_1$, from 0 s to 0.6 s, the voltage magnitude was 220 V (nominal voltage), which remained the same as when $Load_2$ and $Load_3$ were added to the system at 0.6 s to 1.3 s and from 1.3 s to 2 s, respectively. The unchanged voltage magnitude showed that the proposed control scheme tracked the nominal voltage successfully during load changes. So, voltage deviations improved in the proposed control scheme.

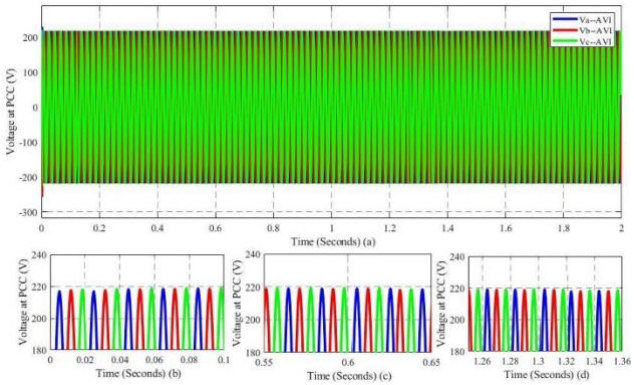

Fig. 9. Voltage magnitude at PCC for three loads in proposed control scheme

The voltage at the PCC for the loads when the system was operating under the SVI-based control scheme is shown in Fig. 10(a). For $Load_1$, the voltage at the PCC was 220 V. After the addition of $Load_2$, the voltage magnitude deviated to 184 V and further deviated to 180 V when $Load_3$ was added to the system, as shown in Figs. 10(b), (c) and (d).

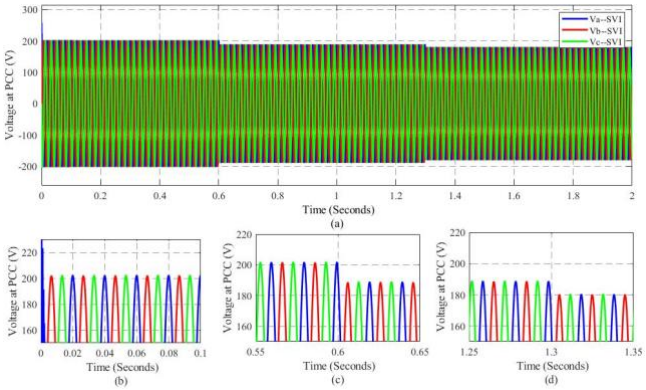

Fig. 10. Voltage magnitude in SVI control scheme

Fig. 11(a) shows the current at the PCC. As shown in the zoomed image in Fig. 11(b), for $Load_1$, the current waveform changed accordingly as per load requirements, and the same cases were observed for $Load_2$ and $Load_3$, as illustrated in the zoomed images in Figs. 11(c) and (d). When $Load_1$ was added to the system between 0–0.6 s, the magnitude of current was 4.1 A. From 0.6 s to 1.3 s, when $Load_2$ was added to the system, the output current at the PCC was 6.4 A, and with the addition of $Load_3$ from 1.3 s to 2 s, the output current was measured at 9.5 A. The output current waveform shows that the magnitude changed with the addition of the loads, which proved that the proposed control scheme worked properly for the connected loads.

Fig. 12(a) shows the current at the PCC for the SVI-based control scheme. As shown in the zoomed image in Fig. 12(b), for $Load_1$, the current waveform changed accordingly as per load requirement, and the same was observed for $Load_2$ and $Load_3$, as illustrated in the zoomed images in Figs. 12(c) and (d).

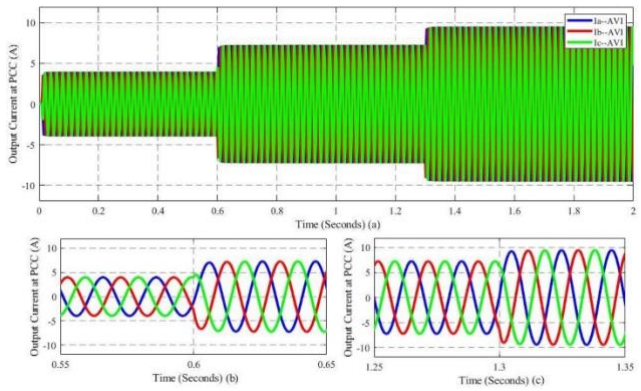

Fig. 11. Output current at PCC with load variation in proposed control scheme

When $Load_1$ was added to the system between 0–0.6 s, the magnitude of current was 3.9 A. From 0.6 s to 1.3 s, when $Load_2$ was added to the system, the output current at the PCC was 5.3 A, and with the addition of $Load_3$ from 1.3 s to 2 s, the output current was measured at 7.9 A.

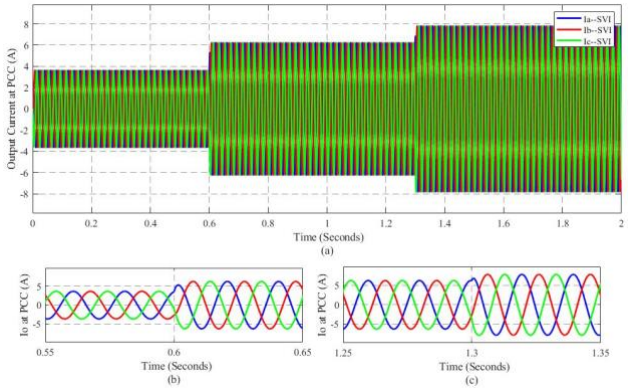

Fig. 12. Output current in SVI control scheme

6. Conclusion

In this paper, improved adaptive-virtual-impedance-based predictive algorithms were proposed to ensure accurate, as well as equal, power sharing as per connected loads. The proposed control algorithms were applied in the MG system with parallel-connected DG inverters and mismatched feeder impedances. Moreover, an adaptive virtual impedance loop was applied with the droop-based control, and the mismatch of the feeder impedances was effectively compensated. A predictive technique was used for signal generation and input prediction. A multi-functioned multi-variable cost function was designed to track the voltage and current signals. The voltage in the proposed control scheme remained constant at the PCC during load changes. Active power *P* and reactive power *Q* were investigated under different load conditions to ensure that the proposed control scheme worked properly, where power sharing was kept updated based on load requirements with constant voltage at the PCC.

Acknowledgments

This research was supported by Universiti Tun Hussein Onn Malaysia (UTHM) through the Multidisciplinary Research Grant (MDR) (H488) and Research Management Centre (RMC) (E 15501).Also thanks to Advanced Control on Power Converter (ACPC) group at FKEE, UTHM.

References

[1] W. Yimin, “Smart Grid and Renewable Energy Profile of SGCC,” Building, pp. 1–9, 2015, [Online]. Available: http://cataleg.upc.edu/record=b1407565~S1*cat.

[2] E. Barklund, N. Pogaku, M. Prodanovic, C. Hernandez-Aramburo, and T. C. Green, “Energy management in autonomous microgrid using stability-constrained droop control of inverters,” IEEE Trans. Power Electron., vol. 23, no. 5, pp. 2346–2352, 2008, doi: 10.1109/TPEL.2008.2001910.

[3] T. Cec et al., “Validation of the CERTS Microgrid Concept,” pp. 1–3, 2006.

[4] B. A. Carreras, D. E. Newman, I. Dobson, and A. B. Poole, “Evidence for self-organized criticality in a time series of electric power system blackouts,” IEEE Trans. Circuits Syst. I Regul. Pap., vol. 51, no. 9, pp. 1733–1740, 2004, doi: 10.1109/TCSI.2004.834513.

[5] K. E. Okedu, A. L. Salmani, and Z. Waleed, “Smart Grid Technologies in Gulf Cooperation Council Countries: Challenges and Opportunities,” Int. J. Smart Grid, vol. 3, no. 2, pp. 92–102, 2019, [Online]. Available: https://www.researchgate.net/profile/Kenneth-Okedu-2/publication/334029620_Smart_Grid_Technologies_in_Gulf_Cooperation_Council_Countries_Challenges_and_Opportunities/links/5d13068092851cf4404c3dff/Smart-Grid-Technologies-in-Gulf-Cooperation-Council-Countr.

[6] F. Ayadi, I. Colak, I. Garip, and H. I. Bulbul, “Impacts of Renewable Energy Resources in Smart Grid,” 8th Int. Conf. Smart Grid, icSmartGrid 2020, pp. 183–188, 2020, doi: 10.1109/icSmartGrid49881.2020.9144695.

[7] A. T. Yee Chong, M. A. Mahmoud, F. C. Lim, and H. Kasim, “A review of Smart Grid Technology, Components, and Implementation,” 2020 8th Int. Conf. Inf. Technol. Multimedia, ICIMU 2020, pp. 166–169, 2020, doi: 10.1109/ICIMU49871.2020.9243430.

[8] J. A. P. Lopes, C. L. Moreira, and A. G. Madureira, “Defining control strategies for analysing microgrids islanded operation,” 2005 IEEE Russ. Power Tech, PowerTech, pp. 1–7, 2005, doi: 10.1109/PTC.2005.4524548.

[9] M. H. Khan, S. A. Zulkifli, E. Pathan, E. Garba, R. Jackson, and H. Arshad, “Decentralize power sharing control strategy in islanded microgrids,” Indones. J. Electr. Eng. Comput. Sci., vol. 20, no. 2, pp. 752–760, 2020, doi: 10.11591/ijeecs.v20.i2.pp752-760.

[10] M. Shafiee-Rad, Q. Shafiee, M. S. Sadabadi, and M. R. Jahed-Motlagh, “Decentralized Voltage Stabilization

and Robust Performance Satisfaction of Islanded Inverter-Interfaced Microgrids," IEEE Syst. J., vol. 15, no. 2, pp. 1893–1904, 2021, doi: 10.1109/JSYST.2020.2994406.

[11] X. Ge, H. Han, W. Xiong, M. Su, Z. Liu, and Y. Sun, "Locally-distributed and globally-decentralized control for hybrid series-parallel microgrids," Int. J. Electr. Power Energy Syst., vol. 116, no. September 2019, p. 105537, 2020, doi: 10.1016/j.ijepes.2019.105537.

[12] Y. Hennane, A. Berdai, J. P. Martin, S. Pierfederici, and F. Meibody-Tabar, "New decentralized control of mesh ac microgrids: Study, stability, and robustness analysis," Sustain., vol. 13, no. 4, pp. 1–25, 2021, doi: 10.3390/su13042243.

[13] A. S. Vijay, N. Parth, S. Doolla, and M. C. Chandorkar, "An Adaptive Virtual Impedance Control for Improving Power Sharing among Inverters in Islanded AC Microgrids," IEEE Trans. Smart Grid, vol. 12, no. 4, pp. 2991–3003, 2021, doi: 10.1109/TSG.2021.3062391.

[14] R. An, Z. Liu, and J. Liu, "Successive-Approximation-Based Virtual Impedance Tuning Method for Accurate Reactive Power Sharing in Islanded Microgrids," IEEE Trans. Power Electron., vol. 36, no. 1, pp. 87–102, 2021, doi: 10.1109/TPEL.2020.3001037.

[15] C. Dou, Z. Zhang, D. Yue, and M. Song, "Improved droop control based on virtual impedance and virtual power source in low-voltage microgrid," IET Gener. Transm. Distrib., vol. 11, no. 4, pp. 1046–1054, 2017, doi: 10.1049/iet-gtd.2016.1492.

[16] T. V. Hoang and H. H. Lee, "Virtual Impedance Control Scheme to Compensate for Voltage Harmonics with Accurate Harmonic Power Sharing in Islanded Microgrids," IEEE J. Emerg. Sel. Top. Power Electron., vol. 9, no. 2, pp. 1682–1695, 2021, doi: 10.1109/JESTPE.2020.2983447.

[17] J. Zhou et al., "Distributed Power Sharing Control for Islanded Single-/Three-Phase Microgrids with Admissible Voltage and Energy Storage Constraints," IEEE Trans. Smart Grid, vol. 12, no. 4, pp. 2760–2775, 2021, doi: 10.1109/TSG.2021.3057899.

[18] J. Lu, M. Zhao, S. Golestan, T. Dragicevic, X. Pan, and J. M. Guerrero, "Distributed Event-triggered Control for Reactive, Unbalanced and Harmonic Power Sharing in Islanded AC Microgrids," IEEE Trans. Ind. Electron., 2021, doi: 10.1109/TIE.2021.3057018.

[19] F. Deng, A. Petucco, P. Mattavelli, and X. Zhang, "An enhanced current sharing strategy for islanded ac microgrids based on adaptive virtual impedance regulation," Int. J. Electr. Power Energy Syst., vol. 134, no. August 2021, p. 107402, 2022, doi: 10.1016/j.ijepes.2021.107402.

[20] S. V. Kulkarni and D. N. Gaonkar, "Improved droop control strategy for parallel connected power electronic converter based distributed generation sources in an Islanded Microgrid," Electr. Power Syst. Res., vol. 201, no. February, p. 107531, 2021, doi: 10.1016/j.epsr.2021.107531.

[21] A. Serrano-Fontova and M. Azab, "Development and performance analysis of a multi-functional algorithm for AC microgrids: Simultaneous power sharing, voltage support and islanding detection," Int. J. Electr. Power Energy Syst., vol. 135, p. 107341, 2022, doi: 10.1016/j.ijepes.2021.107341.

[22] U. N. Patel and H. H. Patel, "Dynamic droop control method for islanded photovoltaic based microgrid for active and reactive power control with effective utilization of distributed generators," Int. J. Renew. Energy Res., vol. 9, no. 2, pp. 1077–1088, 2019.

[23] D. Bai, T. Zhang, and Z. Yang, "Research on Improved Droop Control Strategy of Microsource Inverter Based on Internet of Things," Secur. Commun. Networks, vol. 2021, pp. 1–8, 2021, doi: 10.1155/2021/5043623.

[24] V. E. , Et. al., "Current Harmonics Reduction In Microgrids Using Dual Interfacing Converters," Turkish J. Comput. Math. Educ., vol. 12, no. 2, pp. 1647–1654, 2021, doi: 10.17762/turcomat.v12i2.1450.

[25] B. M. Eid, J. M. Guerrero, A. M. Abusorrah, and M. R. Islam, "A new voltage regulation strategy using developed power sharing techniques for solar photovoltaic generation-based microgrids," Electr. Eng., vol. 103, no. 6, pp. 3023–3031, 2021, doi: 10.1007/s00202-021-01289-3.

[26] B. Liu, Z. Liu, J. Liu, R. An, H. Zheng, and Y. Shi, "An Adaptive Virtual Impedance Control Scheme Based on Small-AC-Signal Injection for Unbalanced and Harmonic Power Sharing in Islanded Microgrids," IEEE Trans. Power Electron., vol. 34, no. 12, pp. 12333–12355, 2019, doi: 10.1109/TPEL.2019.2905588.

[27] S. Vazquez, J. Rodriguez, M. Rivera, L. G. Franquelo, and M. Norambuena, "Model Predictive Control for Power Converters and Drives: Advances and Trends," IEEE Trans. Ind. Electron., vol. 64, no. 2, pp. 935–947, 2017, doi: 10.1109/TIE.2016.2625238.

[28] T. Chen, O. Abdel-Rahim, F. Peng, and H. Wang, "An Improved Finite Control Set-MPC-Based Power Sharing Control Strategy for Islanded AC Microgrids," IEEE Access, vol. 8, pp. 52676–52686, 2020, doi: 10.1109/ACCESS.2020.2980860.

[29] J. Hu, Y. Shan, J. M. Guerrero, A. Ioinovici, K. W. Chan, and J. Rodriguez, "Model predictive control of microgrids – An overview," Renew. Sustain. Energy Rev., vol. 136, no. August 2020, p. 110422, 2021, doi: 10.1016/j.rser.2020.110422.

[30] P. Karamanakos, E. Liegmann, T. Geyer, and R. Kennel, "Model Predictive Control of Power Electronic Systems: Methods, Results, and Challenges," IEEE Open J. Ind. Appl., vol. 1, no. September, pp. 95–114, 2020, doi: 10.1109/ojia.2020.3020184.

[31] R. E. Perez-Guzman, M. Rivera, and P. W. Wheeler, "Recent advances of predictive control in power converters," Proc. IEEE Int. Conf. Ind. Technol., vol. 2020-Febru, pp. 1100–1105, 2020, doi: 10.1109/ICIT45562.2020.9067169.

[32] N. Hamouda, B. Babes, S. Kahla, Y. Soufi, J. Petzoldt, and T. Ellinger, "Predictive Control of a Grid Connected PV System Incorporating Active power Filter functionalities," Proc. - 2019 1st Int. Conf. Sustain. Renew. Energy Syst. Appl. ICSRESA 2019, pp. 0–5, 2019, doi: 10.1109/ICSRESA49121.2019.9182655.

[33] Y. Abdelkader, T. Allaoui, and C. Abdelkader, "Power quality improvement based on five-level shunt APF using sliding mode control scheme connected to a photovoltaic," Int. J. Smart Grid - ijSmartGrid, vol. 1, no. 1, p. 9 Pages, 2017.

[34] J. D. D. Iyakaremye, G. N. Nyakoe, and C. W. Wekesa, "MPC-Based Arctan Droop Control Strategy of the Parallel Inverter System in an Islanded AC Microgrid," J. Eng., vol. 2021, pp. 1–13, 2021, doi: 10.1155/2021/1870590.

[35] A. Navas-Fonseca et al., "Distributed Predictive Secondary Control for Imbalance Sharing in AC Microgrids," IEEE Trans. Smart Grid, vol. 13, no. 1, pp. 20–37, 2022, doi: 10.1109/TSG.2021.3108677.

[36] M. A. Hossain, H. R. Pota, W. Issa, and M. J. Hossain, "Overview of AC microgrid controls with inverter-interfaced generations," Energies, vol. 10, no. 9, pp. 1–27, 2017, doi: 10.3390/en10091300.

[37] J. Singh, S. Prakash Singh, K. Shanker Verma, A. Iqbal, and B. Kumar, "Recent control techniques and management of AC microgrids: A critical review on issues, strategies, and future trends," Int. Trans. Electr. Energy Syst., vol. 31, no. 11, pp. 1–39, 2021, doi: 10.1002/2050-7038.13035.

[38] F. Fang, H. Tian, and Y. Li, "Finite Control Set Model Predictive Control for AC-DC Matrix Converter with Virtual Space Vectors," IEEE J. Emerg. Sel. Top. Power Electron., vol. 9, no. 1, pp. 616–628, 2021, doi: 10.1109/JESTPE.2019.2937330.